HYDROLOGICAL PROCESSES
Hydrol. Process. (2013)
Published online in Wiley Online Library
(wileyonlinelibrary.com) DOI: 10.1002/hyp.9937

Past and future changes in frost day indices in Catskill Mountain region of New York

Aavudai Anandhi,[1]* Mark S. Zion,[2] Prasanna H. Gowda,[3] Donald C. Pierson,[2] David Lounsbury[2] and Allan Frei[4]

[1] *Department of Agronomy, Kansas State University, Manhattan, KS, 66506, USA*
[2] *Water Quality Modeling Group, New York City Department of Environmental Protection, Kingston, NY, USA*
[3] *USDA-ARS Conservation and Production Research Laboratory, Bushland, TX, 79012, USA*
[4] *Department of Geography, Hunter College, City University of New York, New York, NY, USA*

Abstract:

Changes in frost indices in the New York's Catskill Mountains region, the location of water supply reservoirs for New York City, have potentially important implications. Frost day is defined as a day with $T_{min} < 0$ °C. The objective of this study was to investigate past and predicted changes in minimum temperature (T_{min}) and six frost indices in the Catskill Mountains covering six reservoir watersheds. Studied frost indices included (1) number of frost days, (2) number of months with frost, (3) last spring freeze date (LSF), (4) first fall freeze date (FFF), (5) growing season length (GSL), and (6) frost season length. Past changes in the frost indices were studied using observed daily T_{min} for each watershed for the periods 1960–2008. Future changes in frost indices for the periods (2045–2065 and 2080–2100) were studied for emission scenarios (A1B, A2, and B1) downscaled from global climate models (GCMs). Results indicated a general increase in average T_{min} and GSL and a decrease in number of frost days, months with frost, frost season length, earlier LSF, and later FFF from the historical to the future periods, and the magnitude of change varied among the watersheds and GCMs. For the period 1960–2000, in all watersheds (except Cannonsville), LSF occurred earlier by 2.6–4.3 days/decade, FFF occurred later by 2.7–3.2 day/decade, and GSL was longer by 2.4–4 day/decade. Among the scenarios and GCMs, LSF occurred earlier by 4–11 and 4.5–15 days/decade for the periods 2045–2065 and 2081–2100, respectively; FFF occurred later by 1–10 and 4–13 days/decade for the periods 2045–2065 and 2081–2100, respectively; and GSL was longer by 10–25 and 13–40 days/decade for the periods 2045–2065 and 2081–2100, respectively. The increase in GSL is expected to affect hydrologic, ecosystem, and biogeochemical processes with increased net primary productivity and a resulting increase in total annual evapotranspiration. Copyright © 2013 John Wiley & Sons, Ltd.

KEY WORDS Frost day; last spring freeze; first fall freeze; growing season length

Received 28 September 2012; Accepted 10 June 2013

INTRODUCTION

Snow and ice are essential components of the global hydrological and energy cycles, and they are closely associated with the frost occurrence (Jylhä *et al*., 2008). Numerous indices have been used to describe frost's impact on natural and managed ecosystems (Schwartz and Reiter, 2000; Feng and Hu, 2004; Ben-David *et al*., 2010; Zhou and Ren, 2011; Terando *et al*., 2012). Indices make it easier to communicate information about climate anomalies to diverse audiences and allow scientists to assess climate anomalies quantitatively in terms of intensity, duration, frequency, and spatial extent, thereby providing important information useful for planning, designing, and management of applications (Tsakiris and Vangelis, 2005). Commonly used frost indices include the timing of the last frost day in spring and first frost day in fall of each year, number of consecutive frost days, duration of frost-free days, and length of growing season. Many of these indices are calculated using daily minimum air temperature (T_{min}).

Changes in frost indices have important implications in New York's Catskill Mountains region, the location of water supply reservoirs for New York City. More than 90% of the region is covered with forests. Snow is an important component of the region's hydrological systems, ecosystems, infrastructure, travel safety, winter tourism and recreation (Burakowski *et al*., 2008). Studies have shown that an increase in temperature in the region has led to a decrease in snowpack accumulation and duration (Burns *et al*., 2007; Matonse *et al*., 2011; Pradhanang *et al*., 2011; Zion *et al*., 2011). These changes will most likely force changes in the hydrology of the region by decreasing the proportion of precipitation falling as snow, shifting the timing of snowmelt and causing snowmelt-supplemented

*Correspondence to: Aavudai Anandhi, Department of Agronomy, Kansas State University, Manhattan, KS 66506, USA
E-mail: anandhi@ksu.edu

streamflow events to occur earlier in the spring or in late winter, which as a result will decrease the magnitude of traditionally high streamflows in April (Zion *et al.*, 2011). More run-off during winter, in turn, can cause reservoir storage levels, water releases, and spills to increase during the winter and earlier reservoir refill in the spring (Matonse *et al.*, 2011). Changes in last frost day in spring, first frost day in fall, and growing season length (GSL), in turn will change the annual evapotranspiration, streamflow patterns, and the frequency of drought (Huntington *et al.*, 2009). This will have profound direct and indirect effects on forest productivity, nuisance species (including pests, pathogens, and invasive species), wildlife, and forest nutrient cycling (Huntington, 2006; Campbell *et al.*, 2009; Mohan *et al.*, 2009). Hence, investigating current and future climate change on a regional scale is essential to understand potential impacts on humans and the natural environment (Hayhoe *et al.*, 2007). The main objective of this study is to investigate the past and future changes in the frost indices in the Catskill Mountains region of New York State (NY).

STUDY REGION AND DATA

The study region is in the Catskill Mountains, part of the eastern plateau climate region of NY (Figure 1). The study area encompasses an area of about 4100 km^2 and consists of six reservoir watersheds: Cannonsville, Ashokan, Nerversink, Schoharie, Rondout, and Pepacton. The region contributes about 90% of New York City's water supply and has an elevation range of 125–1275 m . These mountainous watersheds are mostly forested with some agricultural land-use (corn, hay, and pasture lands) within the Cannonsville watershed and, to a lesser extent, also within the Schoharie and Pepacton basins. Except for a slight decline in agricultural activity in Cannonsville, there has been little change in land development over the past decade (Schneiderman *et al.*, 2013).

The climate is classified as humid (Keim, 2010) with cool summers (with average minimum, maximum, and mean temperatures of 12, 22, and 18 °C, respectively), colder winters (with average minimum, maximum, and mean temperatures of 0, 10, and 5 °C, respectively), abundant snowfall, and year-round precipitation (Anandhi *et al.* (2011); Figure 2). Typically, total precipitation is about 1000–1200 mm per year, with snowfall accounting for approximately 20% of total precipitation (Anandhi *et al.*, 2011), and snowmelt historically contributes between 24% and 30% of total annual run-off in this region (Schneiderman *et al.*, 2013). The monthly mean snow water equivalent in the six watersheds for December to March are 5.0, 8.1, 9.3, and 2.7 mm/day, respectively (Anandhi *et al.*, 2011). For Cannonsville, the snowfall is ~50 mm/month during winter and contributes about 60% of the total winter precipitation during the 1958–1988 period

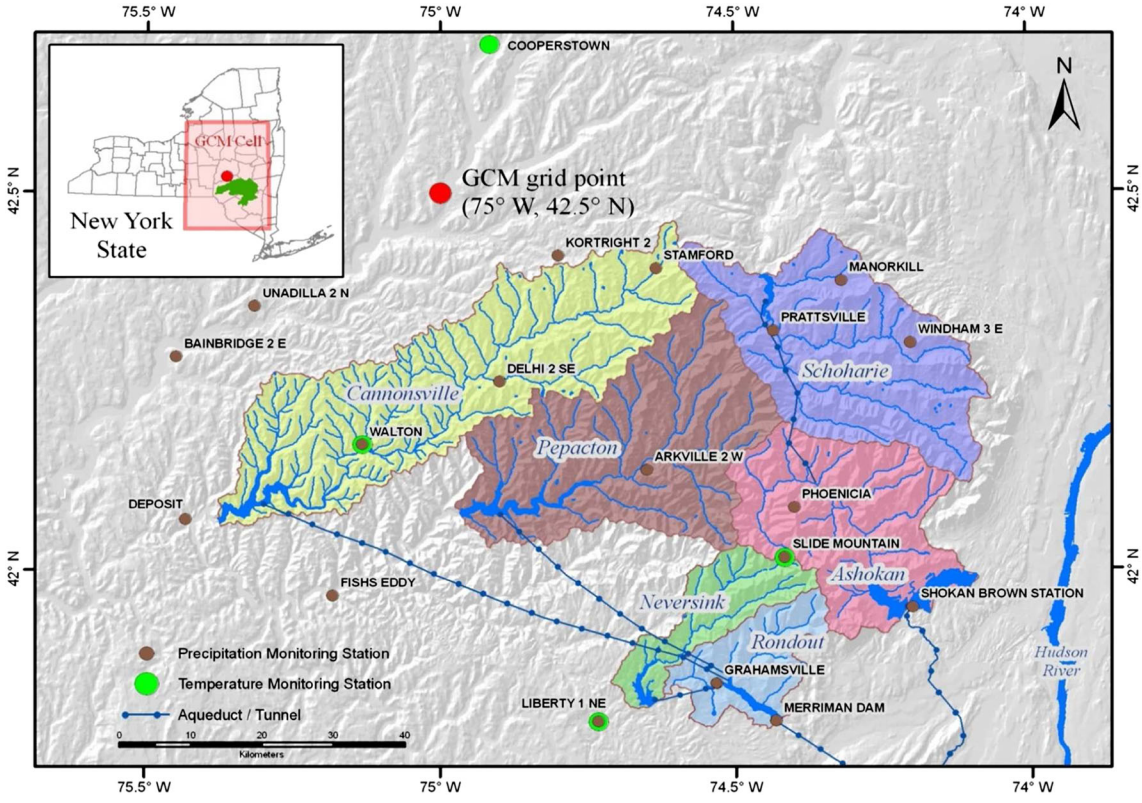

Figure 1. A map of the six reservoir watersheds in the Catskill Mountain region that provides approximately 90% of New York City's drinking water needs. The common grid cell to which all global climate model data were interpolated to is shown in the insert

DOI: 10.1002/hyp

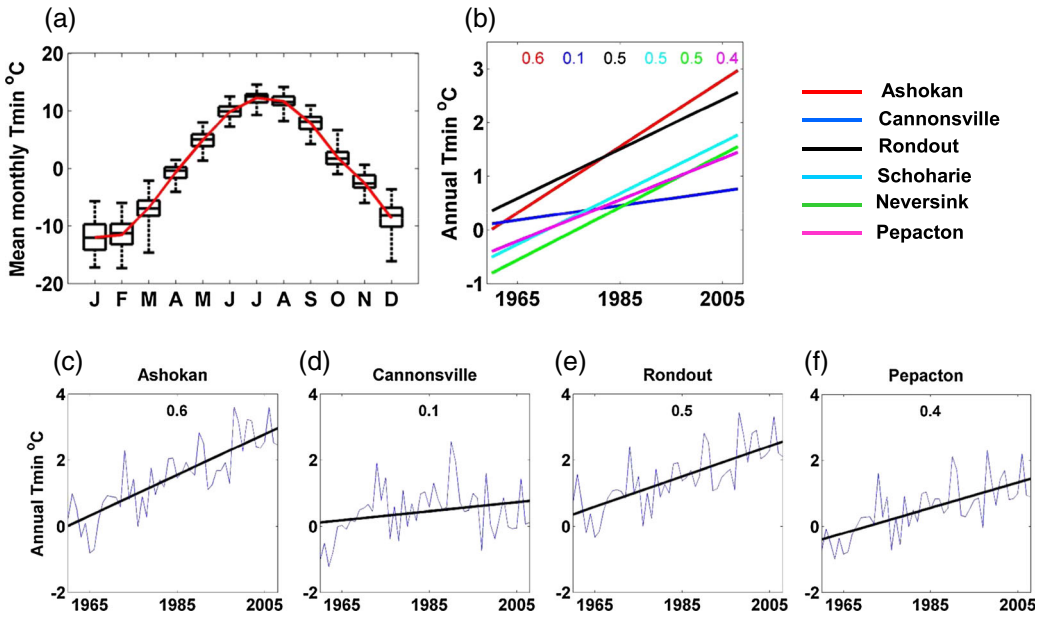

Figure 2. (a) Boxplots of mean monthly T_{min} for the six West of Hudson (WOH) watersheds. Each box is based on 49 years (1960–2008) of data times six watersheds. For this and all subsequent boxplots, the bounds of the box represent the 25th percentile (Q1 quartile) and 75th percentile (Q3 quartile), and the lower whiskers extend from 25th percentile to the minimum value, whereas the upper whisker extends from 75th percentile to the maximum value. The red line is the mean monthly T_{min} for all the six watersheds and all years. (b) Linear trend lines of annual T_{min} calculated as the mean of all daily (January–December) minimum temperatures for each of the six WOH watersheds. (c–f) Linear trend line (black line) and time series plot (blue line) of mean annual T_{min} for each of the six WOH watersheds; the numbers in the top of the subplots (b–f) represent the slope in °C/decade

(Frei *et al*., 2002). Evapotranspiration occurs at a much slower rate during the winter and March and April (periods of spring snowmelt) and occurs the greatest in the summer months with low streamflows (Zion *et al*., 2011).

Observed minimum T_{min} were obtained from the Northeast Regional Climate Center for four stations: Cooperstown, Liberty, Slide Mountain, and Walton (Figure 1), and data for the period 1960–2008 was used in the study. The elevations of these four stations are 366, 472, 808 and 451 m above mean sea level, respectively. Slide Mountain is at a higher elevation when compared with the rest of the stations. Global climate models (GCM) simulations at daily timescale were obtained from the World Climate Research Programme's Coupled Model Intercomparison Project Phase 3 multimodel dataset. The simulations used in the study were for baseline scenario (20C3M), future scenarios (A1B, A2, and B1), and two 21st-century periods (2045–2065 and 2080–2100). A list of the GCM simulations (name and realization number) used in the study is provided in Table I. The data from all the GCMs for the region surrounding the study region were extracted and interpolated to a common 2.5° grid by using bilinear interpolation technique.

Table I. Global climate models, country of origin, and realization numbers for minimum temperatures used in the study

S.N	GCM I.D *	Acronym	T_{min}	Country
1	BCCR-BCM2.0	bcc	1	Norway
2	CGCM3.1(T47)	cc4	1,2,3,4,5	Canada
3	CGCM3.1(T63)	cc6	1	Canada
4	CNRM-CM3	cnr	1	France
5	CSIRO-Mk3.0	cs3	1,2,3	Australia
6	CSIRO-Mk3.5	cs5	1,2,3	Australia
7	ECHAM5/MPI-OM	mpi	1,4	Germany
8	ECHO-G	miu	1,2,3	Germany, Korea
9	FGOALS-g1.0	iap	1,3	China
10	GFDL-CM2.0	gf0	1	USA
11	GFDL-CM2.1	gf1	2	USA
12	GISS-AOM	ga0	1	USA
13	GISS-ER	gir	1	USA
14	INGV-SXG	ing	1	—
15	IPSL-CM4	ips	1,2	France
16	MIROC3.2(hires)	mih	1	Japan
17	MIROC3.2(medres)	mim	1,2,3	Japan
18	MRI-CGCM2.3.2	mri	1,2,3,4,5	Japan
—	Total no. scenarios	—	38	—

*As provided by Lawrence Livermore National Laboratory's Program for Coupled Model Diagnosis and Intercomparison (PCMDI): http://www-pcmdi.llnl.gov/ipcc/model_documentation/ipcc_model_documentation.php.

METHODS

Estimation of daily temperature for a watershed

Frost indices were calculated for the study region (Fig. 1) by using observed and future scenarios of climate inputs. The spatial averaging method includes applying an environmental lapse rate (6 °C/km) to correct for elevation differences between the station and the mean elevation of each reservoir watershed and using inverse

DOI: 10.1002/hyp

distance squared weighting averaging of the four stations (NYCDEP, 2004). A single time series for daily T_{min} for each watershed is obtained after processing the observed T_{min} data from the four observing stations.

Delta change factor methodology

The scenarios of future T_{min} were created using delta change factor methodology. More details of this method can be found in Anandhi *et al*. (2011). In this method, the empirical cumulative distribution function of the simulated baseline (*GCMb*) and future (*GCMf)* climates were estimated. The cumulative distribution function was divided into 25 equal parts (bins), with each bin having four percentile (=100/25). Then, the mean monthly values of *GCMb* and *GCMf* climates were estimated for each bin using Equations (1) and (2).

$$\overline{GCMb_n} = \sum_{i=1}^{Nb} GCMb_{i,n}/Nb \quad (1)$$

$$\overline{GCMf_n} = \sum_{i=1}^{Nf} GCMf_{i,n}/Nf \quad (2)$$

The daily data in a month from all years of a scenario were pooled so *Nb* and *Nf* represent the total number of days associated with a given month during the baseline and future time periods for the *n*th change factor ($n = 1$–25). The *Nb* and *Nf* values varied depending on the month and number of years in the scenario period. Additive change factors associated with each frequency bin ($CF_{add,n}$) were calculated by taking an arithmetic difference between the mean bin value of a GCM variable derived from a current climate simulation and derived for the corresponding bin from a future climate scenario taken at the same GCM grid location (Equation 3). Using the time series of observed local values (*LOb*), pooled monthly data were evaluated to similarly define the range in values associated with each of the 25 bins of the variable frequency distribution. Based on the variable range defining bin (n) during month (m), the appropriate additive change factor was applied to obtain future scaled climate scenarios ($LSf_{add,n,j}$) of the variable for each day (j) of the scenario (Equation 4).

$$CF_{add,n} = \overline{GCMf_n} - \overline{GCMb_n} \quad (3)$$

$$LSf_{add,n,j} = LOb_{n,j} + CF_{add,n} \quad (4)$$

Thus, for each month, 25 CFs are calculated for T_{min} for combinations of GCM, future scenarios (A1B, A2, and B1), and two periods (2045–2065 and 2081–2100) (Table I).

FROST INDICES

A number of definitions of a frost day are available in the literature. In numerous studies, a frost day is defined as a day with a T_{min} less than a base temperature (T_b). Some of the chosen values for T_b are presented in Table IIa. In this study, as with most other studies, a frost day was defined as a day with $T_{min} < 0$ °C ($T_b = 0$ °C). The frost indices used in the study are listed in Table IIb and include the number of frost days (nFDs), number of frost months (nFMs), last spring freeze (LSF), first fall freeze (FFF), GSL, and frost season length (FSL). Trend was estimated using the linear regression method.

RESULTS AND DISCUSSION

Minimum air temperature

Monthly mean daily T_{min} for the six watersheds for the period 1960–2008 is plotted in boxplots in Figure 2a. January had the lowest daily T_{min} values, whereas July recorded the highest value followed closely by August. The range of T_{min} in the boxplots were due to the differences in six watersheds and interannual variations. The range was greatest (10–12 °C) during the winter (December, January, and February), early spring (March), and mid-fall (October), and the difference during the rest of the months was 5–6 °C (Figure 2a). The linear trend lines of the mean annual T_{min} for the six watersheds are plotted in Figures 2b–f. In general, all six watersheds show an increase in T_{min}. Among the watersheds, Cannonsville had the least increase in T_{min} (0.1 °C/decade), and Ashokan had the largest increase (0.6 °C/decade). The differing rates of change in the T_{min} could be due to differences in average elevation and land-use (Table III) between the watersheds.

The oscillations of atmospheric mass between high and midlatitudes are dominant patterns that characterize the northern hemisphere climate variability and are commonly referred to hemispherically as the Arctic Oscillation (AO) and regionally as the North Atlantic Oscillation (NAO) (Gong *et al*., 2002). These oscillations are most prevalent in the winter season and occur over a wide range of timescales, from intraseasonal to interdecadal. The AO exists year-round but is strongest and most variable in winter, and contains expressions in surface air temperatures (Allen and

Table IIa. Frost day definitions and sources

Frost definition	Reference
$T_{min} < 0$ °C	Christidis *et al*., 2007
$T_{min} < -4.4$, –2.2, and 5.6 °C	Robeson 2002
$T_{min} < 2.2$ °C	Schwartz and Reiter, 2000; Goodin *et al*. 1995, 2004
$T_{min} < 2$ °C	Potithep and Yasuoka 2011

DOI: 10.1002/hyp

Table IIb. Definition of the frost indices used in the study

Frost index	Frost index definition
Number of frost days (nFDs)	The number of days with frost
Number of frost months (nFMs)	The number of months with frost
Last spring freeze (LSF)	The last frost (freeze) day is the last day when $T_{min} < 0$ °C in the period starting on 1 March and ending on 30 June.
First fall freeze (FFF)	The first frost (freeze) day is first day when $T_{min} < 0$ °C in the period starting on 1 September and ending on 30 November .
Growing season length (GSL)	The number of days between the LSF and the FFF
Frost season length (FSL)	The number of days between the FFF and the LSF

Table III. General details of the watersheds adapted from Anandhi *et al.* (2011)

S N	Name of reservoir watershed	Elevation range, (mean) m	Watershed area[a] (km^2)	Land-use[b] (%)	
				Forest	Agriculture
1	Ashokan	125–1275 (539)	661	98	1
2	Cannonsville	315–1234 (572)	1177	80	19
3	Neversink	435–1276 (841)	238	98	2
4	Pepacton	353–1181 (633)	961	90	9
5	Rondout	248–1175 (523)	247	96	4
6	Schoharie	315–1234 (632)	817	91	8

[a] Includes the reservoir area.
[b] From Mehaffey *et al.* (2005) (Table I).

Zender, 2010). The positive trend in the winter AO index is associated to warmer winter temperatures in the region in the second half of the 20th century (Overland *et al.*, 2008). At mid to high northern latitudes, the AO statistically explains 31% of the winter temperature and about 40% of the winter temperature trends (Schaefer *et al.*, 2005).

The NAO has been shown to exert a strong influence on climate in eastern North America via latitudinal shifts in the wintertime North Atlantic storm track and associated variations in temperature, precipitation, and cyclonic activity (Gong *et al.*, 2002). For the winter period, the NAO index increased significantly for the period 1948–2001 and has shown to modulate high-frequency (daily) winter climatic variation in high latitude continental regions (Huntington *et al.*, 2004) and influence winter temperatures and precipitation. The positive NAO trends are similar to the AO trends in February and March but different in other months particularly in May and June when NAO trends are negative but AO trends are negligible (Zhou *et al.*, 2001).

Studies have shown that in mountainous terrain such as the study region, the lapse rate vary temporally (e.g. monthly, diurnal, and seasonal cycles) and spatially (e.g. aspect of slope, windward *vs* lee side, location relative to valley, and synoptic types) (Blandford *et al.*, 2008; Minder *et al.*, 2010). However, there is sparsity of long term, high-resolution surface temperature measurements combined with the influences of local factors like cold air pooling and inversions, makes such quantification challenging. Daily T_{min} lapse rates are more variable and tend to be steepest in spring with monthly lapse rate in Idaho during October to April, varied between 0.5 and 3.6 °C/km (Blandford *et al.*, 2008). In another study in Cascade mountain during October to April, the annual mean and seasonal lapse rates in T_{min} were 4.2 °C/km and 4.5–6.0 °C/km, respectively, whereas in the leeward and windward side, the lapse rates were 3.5 to 5.5 °C/km and 2–6.5 °C/km, respectively (Minder *et al.*, 2010). This study assumed a constant environmental lapse rate in estimating the average watershed T_{min}, and so our results are subjective to varying lapse rates.

Boxplots of downscaled future T_{min} for 18 GCMs (Table I), two periods (2045–2065 and 2080–2100), and three special report on emissions scenarios (SRES) (A1B, A2, and B1) are shown in Figure 3 (a, b). In general, all GCMs show an increase in T_{min} except for a few scenarios in June and July for the 2045–2065 period. The magnitude of increase in T_{min} varies with month, GCM, scenario, and time, with a larger increase and range during the period 2080–2100 than in 2045–2065. The increase in T_{min} was 2–3 °C (median values) and 4–6 °C (median values) during the periods 2045–2065 and 2080–2100, respectively. During the 2045–2065 period, winter (December, January, and February) and early spring (March–April) have a greater

DOI: 10.1002/hyp

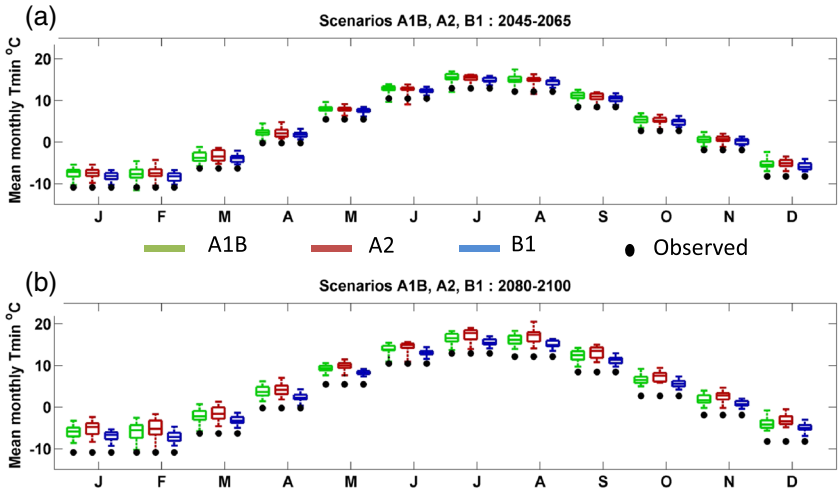

Figure 3. Boxplot of monthly mean downscaled future T_{min} for the six 6 West of Hudson watersheds for 18 global climate models and three emission scenarios (A1B, A2, and B1) for two periods: (a) 2045–2065 and (b) 2080–2100. The daily T_{min} values used to create each box are from multiple scenarios derived from the global climate models in Table I times six watersheds. The black dots in this figure and the red line in the previous figure (2a) represent the monthly mean observed values for the six West of Hudson watersheds

range among GCMs of up to 6 °C. The range of increase among the scenarios also is wider for the period 2080–2100 compared with the period 2045–2065.

Increases in T_{min} during the winter and early spring may influence the timing of snowfall, the number of days of snow cover, frequency of alternating freezing and thawing events, depth, and accumulation and properties of snowpack (Huntington *et al.*, 2009).

NUMBER OF FROST DAYS

The nFDs in a month for the six watersheds for 1960–2008 are plotted in boxplots in Figure 4a. In general, frost occurs in the Catskill Mountains during nine months, September through May; however, a few instances of frost occurred as late as June and as early as August. The variability in nFDs during spring and fall is high compared with the winter months and in general, greatest during the spring of the 1960–2008 historical period. January had the highest nFDs, followed by December, whereas September had the fewest nFDs (median values) during the normal nine-month frost period. The linear trend lines of nFDs in a year for the six watersheds are plotted in Figures 4b–h. In general, all six watersheds show a decrease in nFDs because of a gradual increase in T_{min}. Among the watersheds, Cannonsville showed the lowest decrease in nFDs (−0.3 days/decade), and Ashokan had the highest decrease (−6.6 days/decade). During 1960–2008, on an average, the nFDs in a year for all watersheds in Catskill declined from 177 to 163 days.

Boxplots of nFDs in each month during two future time periods (2045–2065 and 2080–2100) and three SRES scenarios (A1B, A2, and B1) are shown in Figure 5 (a, b). In general, all GCMs showed a decrease in nFDs. The magnitude of the decrease varies with month, GCM, scenario, and time. The differences between A1B and A2 scenarios were less than B1 scenarios during the 2045–2065 period, but during the 2080–2100 period, A2 had the highest decrease followed by A1B and B1 scenarios. The decrease during the period 2080–2100 is generally more than that during the 2045–2065 period, with a median decrease of 5–10 and 8–12 days during the 2045–2065 and 2080–2100 periods, respectively. Winter (December, January, and February) had a lesser decrease in nFDs compared with fall and spring. The range of the decrease is generally wider for 2080–2100 scenarios than for 2045–2065 scenarios.

In mountain valley locations where diurnal temperature ranges can be quite high and the daily average and daily maximum temperatures could conceivably rise in association with greater frequencies of high pressure, while daily minimum temperatures could drop in association with ideal conditions for radiational cooling. Such a scenario could in fact increase the frost indices but result in much lower snowfall and a shorter duration of snow cover. Also, frost (e.g., ice crystals on the vegetation and/or ground surfaces) may still occur even when the 2 m air temperature remains above freezing. So our results are subjective to varying definitions of frost day.

LAST SPRING FROST AND FIRST FALL FROST

Time series and trend lines for LSF and FFF for the six study watersheds are plotted in Figure 6. During 1960–2008, LSF occurred in May in most years (34–39 years out of 49 years) for all six watersheds. LSF occurred in April in about 14–15 years for Ashokan and Rondout watersheds but in June for the remaining four watersheds (7–15 years). All

DOI: 10.1002/hyp

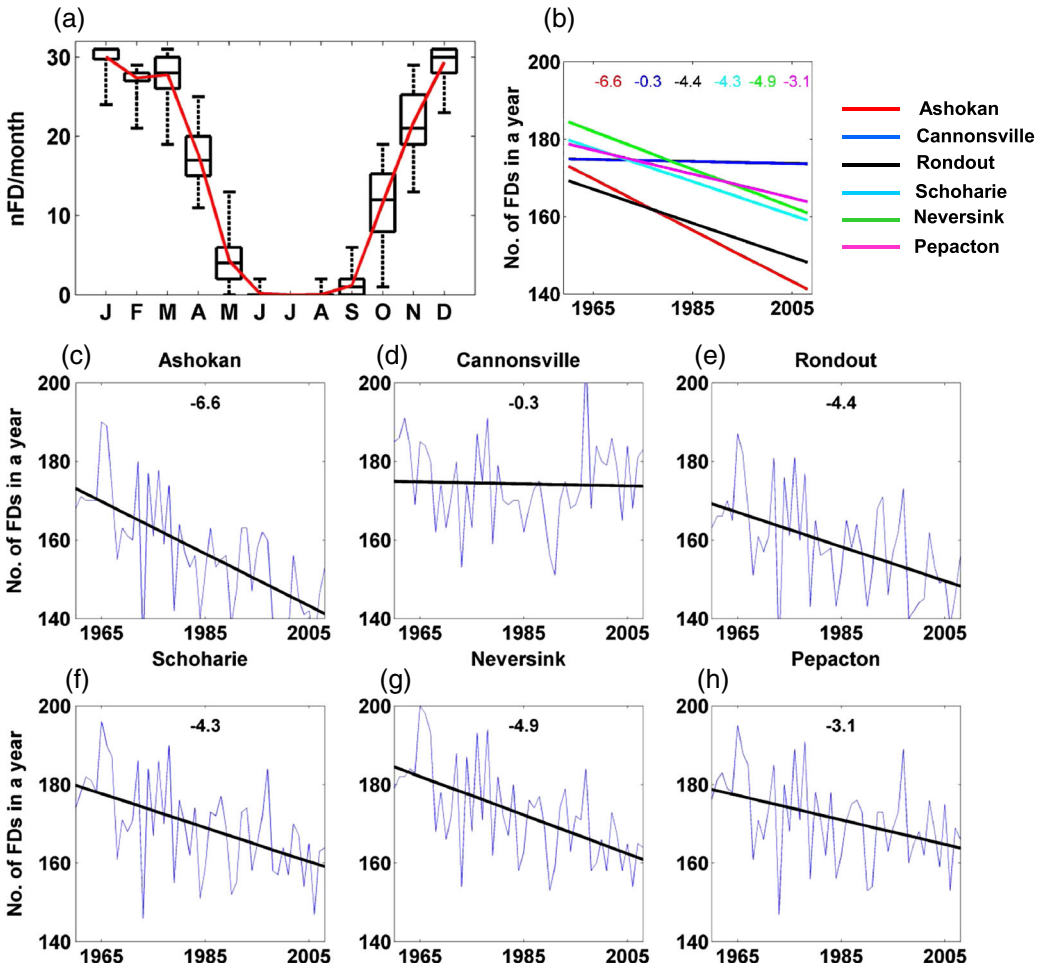

Figure 4. (a) Boxplots of number of frost days (nFDs) in a month for six West of Hudson (WOH) watersheds averaged for 1960–2008. Each box is based on 49 years (1960–2008) of data times six (watersheds) values of nFDs in a year. The red line is the mean nFDs for all six watersheds. (b) Linear trend lines of nFDs for the six WOH watersheds. (c–f) Linear trend line (black line) and time series plot (blue line) of annual nFDs for each of the six WOH watersheds. The numbers in the top of the subplots (b–h) represent the slope in days/decade

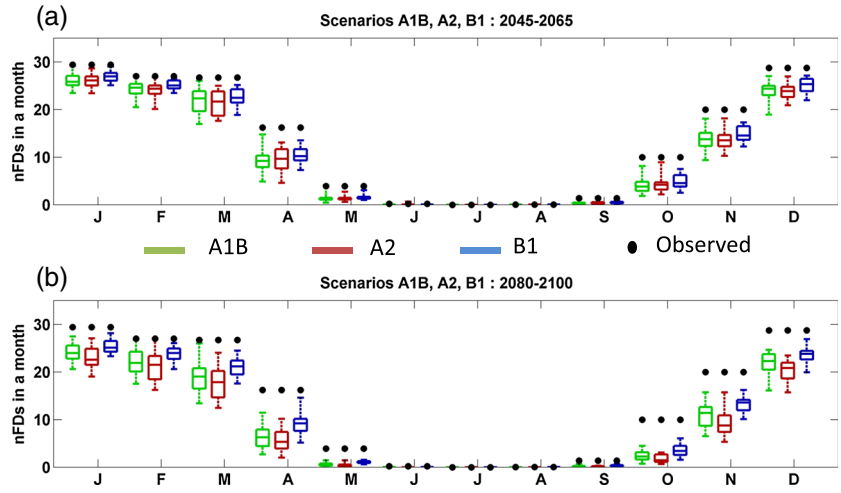

Figure 5. Boxplot of number of frost days in downscaled future T_{min} for six West of Hudson watersheds for three emission scenarios (A1B, A2, and B1) for two periods: (a) 2045–2065 and (b) 2080–2100. Each box is based on the daily data from multiple scenarios derived from the global climate models listed in Table I times six (watersheds). The black dots in this figure and the red line in figure (2a) represent the monthly observed values for the six West of Hudson watersheds

DOI: 10.1002/hyp

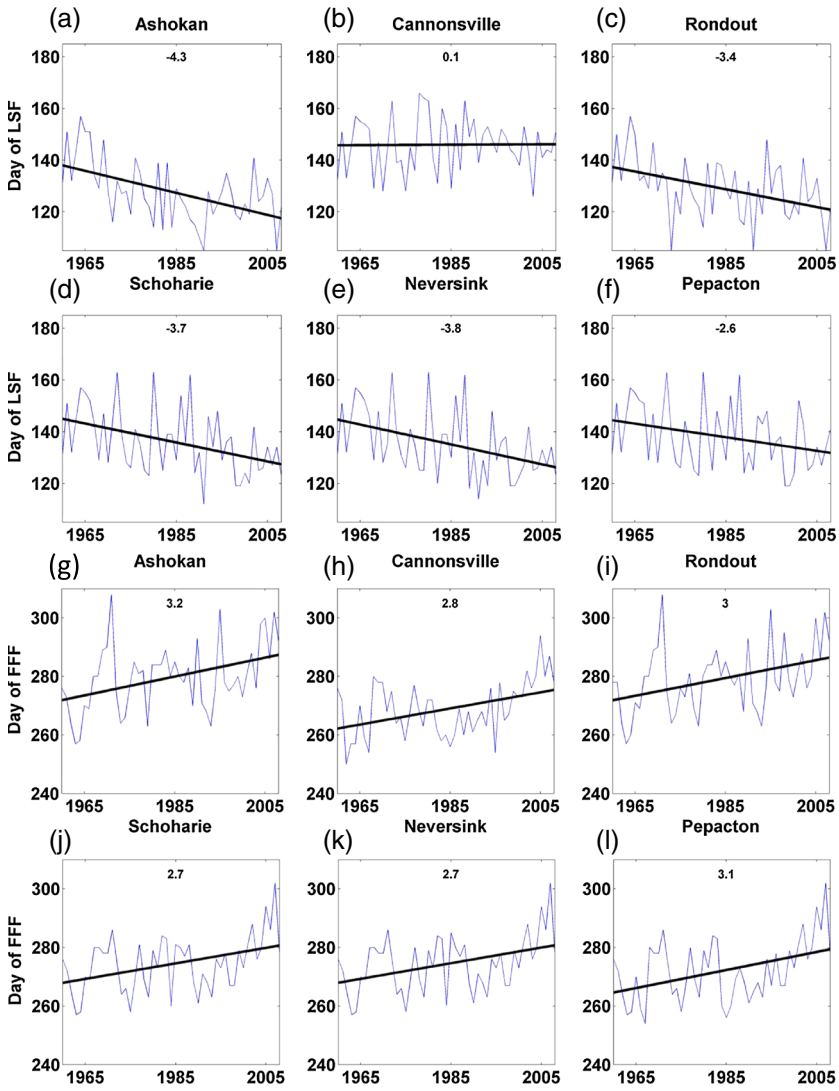

Figure 6. Linear trend line (black line) and time series plot (blue line) for last spring freeze (a–f) and first fall freeze (g–l) for each of the six West of Hudson watersheds. The numbers in the top of the subplots (a–l) represent the slope in days/decade

watersheds except Cannonsville showed a decrease in LSF (−2.6 to −4.3 days/decade; Figure 6a–f), indicating that in general, LSF occurred earlier in the spring season. Cannonsville watershed showed a slight increase of 0.1 day/decade). The earlier occurrence in spring in eastern USA is statistically explained by the increasing trends in the winter AO since the 1960s (Schaefer *et al.*, 2005).

FFF occurred in either October or November in 48 of 49 years for most watersheds. All watersheds experienced an increase in FFF (2.7–3.2 days/decade; Figure 6g–l), indicating that FFF generally occurred later in the fall. The nFMs decreased (figure not shown), with the LSF occurring earlier in the season, and FFF occurring later in the season.

Boxplots of LSF and FFF in future from 18 GCMs for two periods (2045–2065 and 2080–2100) and three SRES scenarios (A1B, A2, and B1) are shown in Figure 7 (a, b). All GCMs showed an earlier LSF and later FFF, which is consistent with historical trends in LSF and FFF. The range of LSF and FFF among the GCMs is higher in 2080–2100 than in 2045–2065 for A1B and A2 emission scenarios. In most GCMs simulations (about 75%), LSF occurred earlier in the spring and FFF occurred later in fall during the 2080–2100. compared to the 2045–2065 period. Among the scenarios and GCMs, LSF occurred earlier by 4–11 and 4.5–15 days / decade for the periods 2045–2065 and 2081–2100, respectively; FFF occurred later by 1–10 and 4–13 days /decade for the periods 2045–2065 and 2081–2100, respectively.

GROWING SEASON LENGTH AND FROST SEASON LENGTH

Time series and trend lines for GSL (Figure 8) and FSL for the six study watersheds are plotted. During the period

DOI: 10.1002/hyp

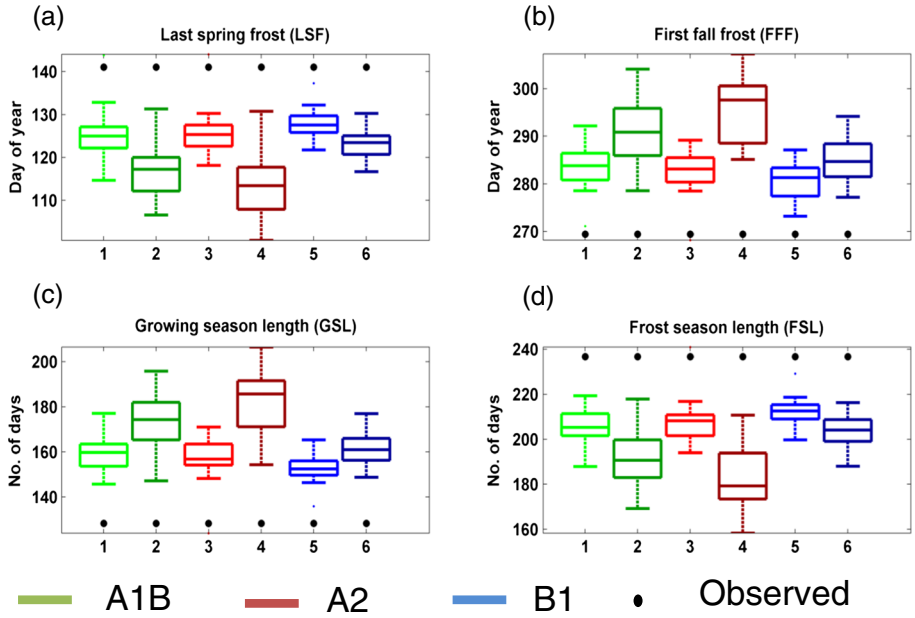

Figure 7. Boxplot of four frost indices (last spring freeze, first fall freeze, growing season length, and frost season length) based on downscaled future values of T_{min} for six West of Hudson watersheds for three emission scenarios (A1B, A2, and B1) for two periods: (a) 2045–2065 (represented as lighter shade) and (b) 2080–2100 (represented as darker shade). Each box is made of ensembles from multiple global climate models explained in Table I times six (watersheds) values. The black dots in this figure represent the mean observed values for the six West of Hudson watersheds. The numbers in the top of subplot (a) represent the slope in days/decade

1960–2008, on an average, the GSL varied from 123–152 days in a year extending from May to late October. All watersheds showed an increase in GSL of about 2.7–7.5 days/decade. With a general increase in GSL, there was a decrease in FSL. On average, the FSL varied from 213–242 days in a year extending from November to May. Among the study watersheds, Cannonsville had the highest FSL (242 days) and least GSL (123 days), whereas Ashokan had the least FSL (213 days) and highest GSL (152 days). Coherent associations between NAO and temperature indices such as nFDs and GSL were observed during 1951–2002 in northeastern USA (Brown *et al.*, 2010), and Cooperstown included in this study was one among the 40 stations used.

Boxplots of GSL and FSL from 18 GCMs for two future periods (2045–2065 and 2080–2100) and three SRES scenarios (A1B, A2, and B1) are shown in Figure 7 (c, d). In general, all GCMs showed a decrease in FSL and an

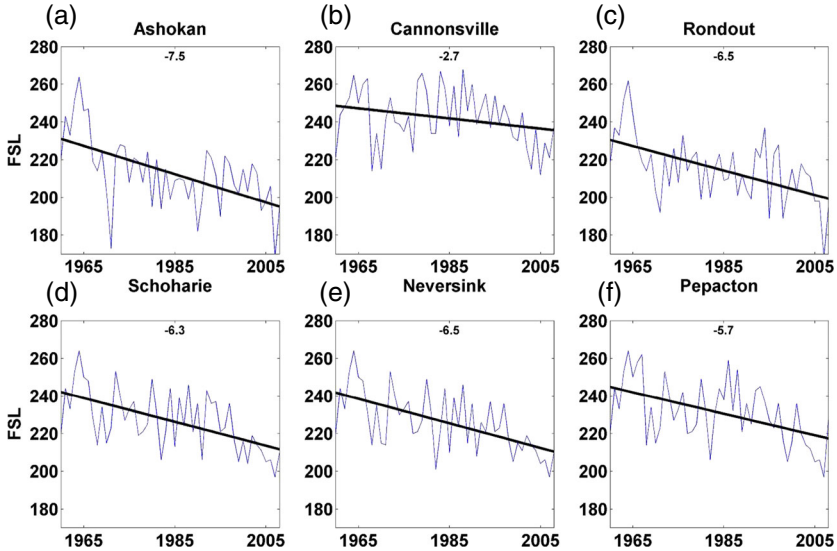

Figure 8. Linear trend line (black line) and time series plot (blue line) for frost season length (a–f) for each of the six West of Hudson watersheds. The numbers in the top of the subplots (a–f) represent the slope in days/decade

DOI: 10.1002/hyp

increase in GSL and were consistent with historical trends. The range in the FSL values obtained among the GCMs was higher in 2080–2100 than in 2045–2065 for A1B and A2 emission scenarios. For most GCMs (about 75 percentile), GSL is longer and FSL is shorter for period 2080–2100 than for 2045–2065. Among the scenarios and GCMs, GSL was longer by 10–25 day /decade and 13–40 days /decade for the periods 2045–2065 and 2081–2100, respectively, and FSL was shorter by the same rate for the two periods.

Increase in GSL will generally lead to an increase in annual evapotranspiration, and changes in LSF and FFF affect phenological events in the region such as bud break in spring and senescence and dormancy in the fall. The decrease in soil moisture during the growing season in substantial parts of eastern USA is likely attributed to increase in evapotranspiration and GSL rather than decreases in rainfall because the historical data do not suggest a decrease in summer rainfall during 1950–2000 period (Huntington *et al*., 2009).

Some of the possible reasons for the variability in the frost indices are discussed. Among the four stations used in the study, Slide Mountain has a higher increase in T_{min} and is at a higher elevation when compared with the rest. While estimating T_{min} for each watershed (using inverse distance squared weighting averaging), Cannonsville is least influenced by Slide Mountain. Also, little change in land development over the past decade is observed in the watershed (Schneiderman *et al*., 2013). Further, Ashokan watershed has a higher precipitation than Cannonsville watershed because of the south-east to north-west precipitation gradient across the region and the high elevation of the Slide Mountain station (Frei *et al*., 2002). The total evapotranspiration in Cannonsville and Askokan are comparable, but the percentage of total precipitation lost as total evapotranspiration is higher for Cannonsville (60%) when compared with Ashokan (30-45%) because the precipitation gradient (Frei *et al*., 2002). However the changes in GSL could change the total evapotranspiration and the period of low streamflow in the region.

Our results add local precision to the earlier findings that encompassed larger areas (Schwartz and Reiter, 2000; Adger *et al*., 2003; Kiktev *et al*., 2003; Feng and Hu, 2004; Christidis *et al*., 2007; Hayhoe *et al*., 2007; Trenberth *et al*., 2007; Hayhoe *et al*., 2008). Earlier LSF, later FFF, and longer GSL could affect the hydrologic, ecosystem, and biogeochemical processes both positively and negatively (Huntington, 2006; Campbell *et al*., 2009; Mohan *et al*., 2009).

CONCLUSION

Overall, our results indicated a general increase in average annual T_{min} and GSL, a decrease in the number of frost-free days (nFFDs) and FSL, earlier occurrence of LSF, and later occurrence of FFF. These trends were detected in the historical record (1960–2008) and were also seen in comparisons between baseline and future climate scenarios. For the period 1960–2000, in all watersheds (except Cannonsvelle), LSF occurred earlier by 2.6–4.3 days/decade, FFF occurred later by 2.7–3.2 days/decade, and GSL was longer by 2.6–7.5 days/decade. The variability in the trends in the frost indices among the watersheds could be due to the variability among the stations, watershed elevation differences, south-east to north-west precipitation gradient across the region, and land development over the past decade in certain regions. The trends in the frost indices are also subjective to varying periods for which the analysis is carried out.

The direction of change in frost indices estimated from the GCM simulations in the region were the same in almost all the scenarios and time periods, however, the magnitude of change varied among the GCMs. A2 scenario during the period 2081–2100 showed a greater change compared to the other emission scenarios. Among the scenarios and GCMs, LSF occurred earlier by 4–11 days /decade and 4.5–15 days /decade for the periods 2045–2065 and 2081–2100, respectively; FFF occurred later by 1–10 days / decade, and 4–13 days /decade for the periods 2045–2065 and 2081–2100, respectively; GSL was longer by 10–25 day /decade and 13–40 days /decade for the periods 2045–2065 and 2081–2100, respectively. Our results add local precision to the earlier findings that encompassed larger areas (Schwartz and Reiter, 2000; Adger *et al*., 2003; Kiktev *et al*., 2003; Feng and Hu, 2004; Christidis *et al*., 2007; Hayhoe *et al*., 2007; Trenberth *et al*., 2007; Hayhoe *et al*., 2008). Some of the implications of these changes in the Catskill Mountains region are discussed.

However, one should be aware that this study assumes a constant environmental lapse rate in estimating the frost indices, and the errors associated with this assumption is unquantified but may be quite important. Also, these results are subjective to the different definitions of frost indices. In future, it would be interesting to correlate the changes in frost indices with the changes in snow statistics and number of days with snow. Also, in future, it would be interesting to study the impact of the changes in GSL on evapotranspiration and the period of low streamflow. Further in-depth study is necessary to understand the direct and indirect effects of these changes on forest productivity, nuisance species (pests, pathogens, and invasive species), wildlife, and forest nutrient cycling.

ACKNOWLEDGEMENTS

This material is based upon work supported by the National Science Foundation under Award No. EPS-0903806 and matching support from the State of Kansas through Kansas Technology Enterprise Corporation. This is the contribution

DOI: 10.1002/hyp

number 13-073-J from the Kansas Agricultural Experiment Station. We thank the anonymous reviewers for helpful and constructive comments and suggestions.

REFERENCES

Adger WN, Huq S, Brown K, Conway D, Hulme M. 2003. Adaptation to climate change in the developing world. *Progress in Development Studies* **3**: 179–195. DOI: 10.1191/1464993403ps060oa.

Allen R, Zender C. 2010. Effects of continental-scale snow albedo anomalies on the wintertime Arctic oscillation. *Journal of Geophysical Research-Atmospheres* **115**: D23105.

Anandhi A, Frei A, Pradhanang SM, Zion MS, Pierson DC, Schneiderman EM. 2011. AR4 climate model performance in simulating snow water equivalent over Catskill Mountain watersheds, New York, USA. *Hydrological Processes* **25**: 3302–3311. DOI: 10.1002/hyp.8230.

Ben-David R, Abbo S, Berger J. 2010. Stress gradients select for ecotype formation in Cicer judaicum Boiss, a wild relative of domesticated chickpea. *Genetic Resources and Crop Evolution* **57**: 193–202. DOI: 10.1007/s10722-009-9461-z.

Blandford TR, Humes KS, Harshburger BJ, Moore BC, Walden VP, Ye H. 2008. Seasonal and synoptic variations in near-surface air temperature lapse rates in a mountainous basin. *Journal of Applied Meteorology and Climatology* **47**: 249–261.

Brown PJ, Bradley RS, Keimig FT. 2010. Changes in extreme climate indices for the northeastern United States, 1870–2005. *Journal of Climate*, **23**: 6555–6572. DOI: 10.1175/2010jcli3363.1.

Burakowski EA, Wake CP, Braswell BH, Brown DP. 2008. Trends in wintertime climate in the northeast United States, 1965–2005. *Journal of Geophysical Research* **113**: D20114. DOI: DOI:10.1029/2008JD009870.

Burns DA, Klaus J, McHale MR. 2007. Recent climate trends and implications for water resources in the Catskill Mountain Region, New York, USA. *Journal of Hydrology* **336**: 155–170.

Campbell JL, Rustad LE, Boyer EW, Christopher SF, Driscoll CT, Fernandez IJ, Groffman PM, Houle D, Kiekbusch J, Magill AH, Mitchell MJ, Ollinger SV. 2009. Consequences of climate change for biogeochemical cycling in forests of northeastern North America. This article is one of a selection of papers from NE Forests 2100: A synthesis of climate change impacts on forests of the Northeastern US and Eastern Canada. *Canadian Journal of Forest Research* **39**: 264–284. DOI: 10.1139/x08-104.

Christidis N, Stott PA, Brown S, Karoly DJ, Caesar J. 2007. Human contribution to the lengthening of the growing season during 1950–99. *Journal of Climate* **20**: 5441–5454. DOI: 10.1175/2007jcli1568.1.

Feng S, Hu Q. 2004. Changes in agro-meteorological indicators in the contiguous United States: 1951–2000. *Theoretical and Applied Climatology* **78**: 247–264. DOI: 10.1007/s00704-004-0061-8.

Frei A, Armstrong RL, Clark MP, Serreze MC. 2002. Catskill Mountain water resources: vulnerability, hydroclimatology, and climate-change sensitivity. *Annals of the Association of American Geographers* **92**: 203–224.

Gong G, Entekhabi D, Cohen J. 2002. A large-ensemble model study of the wintertime AO-NAO and the role of interannual snow perturbations. *Journal of Climate* **15**: 3488–3499.

Goodin DG, Mitchell JE, Knapp MC, Bivens RE. 1995, 2004. Climate and weather atlas of Kansas. Kansas Geological Survey Publications Educational series 12.

Hayhoe K, Wake C, Huntington T, Luo L, Schwartz M, Sheffield J, Wood E, Anderson B, Bradbury J, DeGaetano A, Troy T, Wolfe D. 2007. Past and future changes in climate and hydrological indicators in the US Northeast. *Climate Dynamics* **28**: 381–407. DOI: 10.1007/s00382-006-0187-8.

Hayhoe K, Wake C, Anderson B, Liang X-Z, Maurer E, Zhu J, Bradbury J, DeGaetano A, Stoner A, Wuebbles D. 2008. Regional climate change projections for the Northeast USA. *Mitigation and Adaptation Strategies for Global Change* **13**: 425–436. DOI: 10.1007/s11027-007-9133-2.

Huntington TG. 2006. Evidence for intensification of the global water cycle: review and synthesis. *Journal of Hydrology* **319**: 83–95. DOI: 10.1016/j.jhydrol.2005.07.003.

Huntington TG, Hodgkins GA, Keim BD, Dudley RW. 2004. Changes in the proportion of precipitation occurring as snow in New England (1949–2000). *Journal of Climate* **17**: 2626–2636.

Huntington TG, Richardson AD, McGuire KJ, Hayhoe K. 2009. Climate and hydrological changes in the northeastern United States: recent trends and implications for forested and aquatic ecosystems This article is one of a selection of papers from NE Forests 2100: a synthesis of climate change impacts on forests of the Northeastern US and Eastern Canada. *Canadian Journal of Forest Research* **39**: 199–212.

Jylhä K, Fronzek S, Tuomenvirta H, Carter T, Ruosteenoja K. 2008. Changes in frost, snow and Baltic sea ice by the end of the twenty-first century based on climate model projections for Europe. *Climatic Change* **86**: 441–462. DOI: 10.1007/s10584-007-9310-z.

Keim B. 2010. The lasting scientific impact of the Thronthwaite water-balance model. *Geographical Review* **100**: 295–300.

Kiktev D, Sexton DMH, Alexander L, Folland CK. 2003. Comparison of modeled and observed trends in indices of daily climate extremes. *Journal of Climate* **16**: 3560–3571.

Matonse AH, Pierson DC, Frei A, Zion MS, Schneiderman EM, Anandhi A, Mukundan R, Pradhanang SM. 2011. Effects of changes in snow pattern and the timing of runoff on NYC water supply system. *Hydrological Processes* **25**: 3278–3288. DOI: 10.1002/hyp.8121.

Minder JR, Mote PW, Lundquist JD. 2010. Surface temperature lapse rates over complex terrain: lessons from the Cascade Mountains. *Journal of Geophysical Research* **115**: D14122.

Mohan J, Cox R, Iverson L. 2009. Northeastern forest composition and productivity in a future, warmer world. *Canadian Journal of Forest Research* **39**: 213–230.

NYCDEP. 2004. *"Multi Tiered" Water Quality Modeling Program Semi-Annual Status Report—EPA Filtration Avoidance Deliverable Report*. New York City Department of Environmental Protection (NYCDEP): Valhalla, NY.

Overland J, Wang M, Salo S. 2008. The recent Arctic warm period. *Tellus A* **60**: 589–597.

Pradhanang SM, Anandhi A, Mukundan R, Zion MS, Pierson DC, Schneiderman EM, Matonse A, Frei A. 2011. Application of SWAT model to assess snowpack development and streamflow in the Cannonsville watershed, New York, USA. *Hydrological Processes* **25**: 3268–3277. DOI: 10.1002/hyp.8171.

Potithep S, Yasuoka Y. 2011. Application of the 3-PG model for gross primary productivity estimation indeciduous broadleaf forests: a study area in Japan. *Forests* **2**(2): 590–609.

Robeson SM. 2002. Increasing growing-season length in Illinois during the 20th century. *Clim Chang* **52**(1): 219–238. DOI: 10.1023/a:1013088011223.

Schaefer K, Denning AS, Leonard O. 2005. The winter Arctic Oscillation, the timing of spring, and carbon fluxes in the Northern Hemisphere. *Global Biogeochemical Cycles* **19**: GB3017.

Schneiderman EM, Matonse AH, Zion MS, Lounsbury DG, Mukundan R, Pradhanang SM, Pierson DC. 2013. Comparison of approaches for snowpack estimation in New York City watersheds. *Hydrological Processes*: n/a-n/a. DOI: 10.1002/hyp.9868.

Schwartz MD, Reiter BE. 2000. Changes in North American spring. *International Journal of Climatology* **20**: 929–932.

Terando A, Easterling W, Keller K, Easterling D. 2012. Observed and modeled twentieth-century spatial and temporal patterns of selected agro-climate indices in North America. *Journal of Climate* **25**: 473.

Trenberth K, Jones P, Ambenje P, Bojariu R, Easterling D, Klein Tank A, Parker D, Rahimzadeh F, Renwick J, Rusticucci M, Soden B, Zhai P. 2007. Observations: surface and atmospheric climate change. In Climate Change 2007: The Physical Science Basis. Contribution of Working Group I to the Fourth Assessment Report of the Intergovernmental Panel on Climate Change. Solomon S, Qin D, Manning M, Chen Z, Marquis M, Averyt K, Tignor M, Miller H (eds.).

Tsakiris G, Vangelis H. 2005. Establishing a drought index incorporating evapotranspiration. *European Water* **9–10**: 1–9.

Zhou Y, Ren G. 2011. Change in extreme temperature event frequency over mainland China, 1961–2008. *Climate Research* **50**: 125–139.

Zhou S, Miller AJ, Wang J, Angell JK. 2001. Trends of NAO and AO and their associations with stratospheric processes. *Geophysical Research Letters* **28**: 4107–4110. DOI: 10.1029/2001gl013660.

Zion MS, Pradhanang SM, Pierson DC, Anandhi A, Lounsbury DG, Matonse AH, Schneiderman EM. 2011. Investigation and modeling of winter streamflow timing and magnitude under changing climate conditions for the Catskill Mountain region, New York, USA. *Hydrological Processes* **25**: 3289–3301. DOI: 10.1002/hyp.8174.